Polyhedron 101 (2015) 93–102

Contents lists available at ScienceDirect

Polyhedron

journal homepage: www.elsevier.com/locate/poly

Nickel(II) complexes having different configurations controlled by N,N,O-donor Schiff-base ligands in presence of isothiocyanate as co-ligand: Synthesis, structures, comparative biological activity and DFT study

Jaydeep Adhikary [a], Priyanka Kundu [a], Sanchari Dasgupta [a], Sudeshna Mukherjee [b], Sreya Chattopadhyay [b], Gabriel Aullón [c], Debasis Das [a,*]

[a] Department of Chemistry, University of Calcutta, 92 A. P. C. Road, Kolkata 700 009, India
[b] Department of Physiology, University of Calcutta, 92 A. P. C. Road, Kolkata 700 009, India
[c] Departament de Química Inorgànica and Institut de Química Teòrica i Computacional, Universitat de Barcelona, Martí i Franquès 1-11, 08028 Barcelona, Spain

ARTICLE INFO

Article history:
Received 5 June 2015
Accepted 20 July 2015
Available online 26 July 2015

Keywords:
Schiff base Ni(II) complex
Square planar and octahedral geometry
DFT study
Bioactivity

ABSTRACT

Four mononuclear nickel(II) complexes, *viz.* $[NiL^1(OAc)(H_2O)_2]\cdot 2H_2O$ (**1**), $[NiL^1(NCS)(H_2O)_2]\cdot H_2O$ (**1a**), $[NiL^2(OAc)(H_2O)]$ (**2**), and $[NiL^2(NCS)]$ (**2a**) (where HL^1 = 2-[(2-Morpholin-4-yl-ethylimino) -methyl]-phenol and HL^2 = 2-[(2-Pyrrolidin-1-yl-ethylimino)-methyl]-phenol) have been synthesized and structurally characterized. Single crystal X-ray analysis reveals the presence of square planar coordination geometry about nickel for **2a**, whereas others have distorted octahedral geometry. DFT calculations have done to explore the origin of different geometries of **1a** and **2a** although their preparative procedure is same. The influence of different geometries *i.e.*, octahedral and square-planar on the anticancer activity of Ni(II) have been investigated on Erhlich's ascities carcinoma (EAC) cells and the order of anticancer activity is **2a** > **1a** > **2** > **1**. The biological results are further compared to the activity of *cis*-platin.

1. Introduction

Nickel(II) has very rich coordination chemistry owing to its inherent ability to espouse various geometries [1–7]. This versatile coordination chemistry of nickel has an area of considerable importance in inorganic chemistry with implications in other areas of chemistry and biology [8–10]. Schiff base complexes present suitable biometric properties that can mimic the structural features of the active sites, and they have been extensively used in various fields such as disease treatment, biochemical reaction and biological regulator [11–14]. Some articles about the interaction of DNA with macrocyclic Schiff base nickel(II) complex have been reported [15–18]. In our lab octahedral Ni(II) Schiff base complexes have been widely studied in various biological field [19]. But the activity of square planar Ni(II) complex is yet to explore in biological study. For this purpose, we have prepared octahedral Ni(II) complexes (**1** and **2**) of two closely related Schiff base ligands (HL^1 and HL^2). Further treatment of **1** and **2** with sodium thoicyanate produce octahedral **1a** and square planar **2a**, respectively (Scheme 1). We have tried to explain the origin of such transformation from octahedral **2** to square planar **2a** by DFT calculation. Anticancer activity of all the complexes has been studied on Erhlich's ascities carcinoma cell. All the four complexes show excellent anticancer activity. ROS generation is responsible for such activity. DNA fragmentation activity of the complexes has been proved by fluorescence imaging. Experimental outcome suggest that square planar complex (**2a**) is the most efficient among the all. This can be explained as the high penetration property due to planarity as reported previously [20–22]. Cytotoxicity result of the complexes corroborates that toxicity level is lesser towards normal cell in compare to cancer cell.

2. Experimental

2.1. Physical methods and materials

Elemental analyses (carbon, hydrogen and nitrogen) were performed using a Perkin–Elmer 240C elemental analyzer. Infrared spectra (4000–500 cm^{-1}) were recorded at 27 °C using a Perkin–Elmer RXI FT-IR spectrophotometer with KBr pellets. Electronic spectra (1400–200 nm) were obtained at 27 °C using a Shimadzu

* Corresponding author.
E-mail address: dasdebasis2001@yahoo.com (D. Das).

http://dx.doi.org/10.1016/j.poly.2015.07.055
0277-5387/

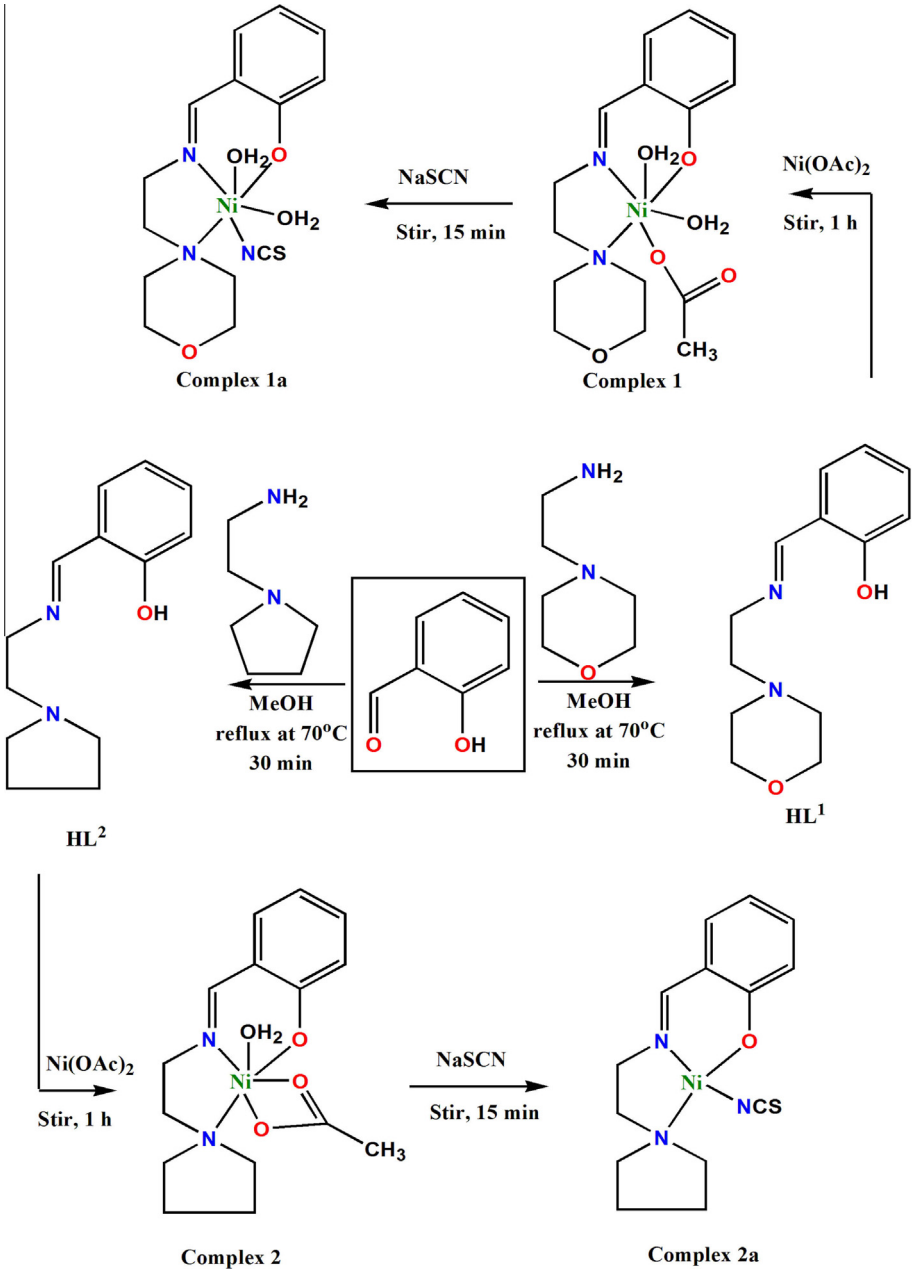

Scheme 1. Schematic route of complexes.

UV-3101PC with methanol as solvent and reference. Thermal analyses (TG–DTA) were carried out on a Mettler Toledo (TGA/SDTA851) thermal analyzer in flowing dinitrogen (flow rate: 30 cm^3 min^1). Ambient temperature magnetic susceptibility measurements were performed with Magway MSB Mk1 magnetic susceptibility balance. All chemicals were obtained from commercial sources and used as received. Solvents were dried according to standard procedure and distilled prior to use. Salicylaldehyde, N-(2-aminoethyl) morpholine, N-(2-aminoethyl) pyrolidine, Nickel(II) acetate hexahydrate and Sodium thiocyanate were purchased from Aldrich.

2.2. Synthesis of complexes

2.2.1. Synthesis of Complex $[NiL^1(OAc)(H_2O)_2]\cdot 2H_2O$ (**1**)

A methanolic solution (5 mL) of N-(2-aminoethyl) morpholine (0.260 g, 2 mmol) was added dropwise to a hot methanolic solution (10 mL) of salicylaldehyde (0.244 g, 2 mmol) and the resulting solution was refluxed for 30 min. Then, methanolic solution (5 mL) of Nickel acetate (0.497 g, 2 mmol) was added and resulting solution was stirred for 1 h. The green solution was filtered, kept in a $CaCl_2$ desiccator in dark and after a few days crystals of complex **1**, suitable for X-ray data analysis were obtained. (Yield 73%). *Anal.* Calc. for $C_{30}H_{54}N_4Ni_2O_{15}$: C, 43.47; H, 6.52; N, 6.67. Found: C, 43.41; H, 6.49; N, 6.62%. UV–Vis–NIR (methanol, nm) λ_{max} = 621, 758, 949.

2.2.2. Synthesis of Complex $[NiL^1(NCS)(H_2O)_2]\cdot H_2O$ (**1a**)

After following the same procedure as for **1** aqueous solution of Sodium thiocyanate (0.162 g, 2 mmol) was added to it and the solution was stirred for more 15 min. Resulting green solution was filtered, kept in a $CaCl_2$ desiccator. Few days later green single crystals of **1a** were obtained, suitable for X-ray data collection. (Yield 79%). *Anal.* Calc. for $C_{14}H_{23}N_3NiO_5S$: C, 41.58; H, 5.69; N,

Table 1
Crystallographic data and details of structure refinement for the complexes.

	1	1a	2	2a
Empirical formula	$2(C_{15}H_{24}N_2NiO_6)$, $3(H_2O)$	$C_{14}H_{21}N_3NiO_4S$, H_2O	$C_{15}H_{22}N_2NiO_4$	$C_{14}H_{17}N_3NiOS$
Formula mass	828.15	404.11	353.04	334.07
Crystal system	monoclinic	triclinic	triclinic	monoclinic
Space group	$C2/c$ (No. 15)	$P\bar{1}$ (No. 2)	$P\bar{1}$ (No. 2)	$P21/n$ (No.14)
a (Å)	25.2737(16)	8.7824(3)	9.5340(3)	10.182(5)
b (Å)	9.6509(6)	9.6530(3)	11.1002(3)	18.687(5)
c (Å)	16.6677(11)	11.5092(4)	16.7590(5)	16.093(5)
α (°)	90	95.749(1)	74.277(1)	90
β (°)	110.885(2)	90.179(2)	75.438(1)	105.660(5)
γ (°)	90	111.469(1)	70.363(1)	90
V (Å^3)	3798.4(4)	902.61(5)	1582.59(8)	2948.4(19)
Z	4	2	4	8
T (K)	293	293	293	293
μ (Mo Kα) (mm^{-1})	1.062	1.218	1.482	1.456
D_{calc} (g cm^{-3})	1.448	1.487	1.245	1.505
$F(000)$	1752	424	744	1392
θ max (°)	26.9	34.0	32.9	29.1
Total, Unique Data (R_{int})	21880, 4066 (0.029)	13312, 6819 (0.018)	28951, 11098 (0.023)	44749, 7823 (0.038)
Observed ($I > 2\sigma(I)$)	3480	5831	8190	5813
N_{ref}, N_{par}	4066, 259	6819, 241	11098, 413	7823, 361
R, wR_2, S	0.0335, 0.0920, 1.04	0.0327, 0.0916, 0.98	0.0393, 0.1810, 0.70	0.0365, 0.1024, 0.97
Residual extrema (e Å^{-3})	−0.35, 0.75	−0.37, 0.54	−0.37, 0.65	−0.77, 0.41

10.39. Found: C, 41.56; H, 5.64; N, 10.35%. UV–Vis–NIR (methanol, nm) λ_{max} = 612, 755, 916.

2.2.3. Synthesis of Complex [NiL^2(OAc)(H$_2$O)] (**2**)

Complex **2** was synthesized by following exact procedure as mentioned for complex **1**. Here N-(2-aminoethyl)pyrolidine (0.228 g, 2 mmol) was used in place of N-(2-aminoethyl) morpholine in time of Schiff base preparation. X ray diffractable green crystals of complex **2** were obtained from the final solution after one week (Yield 76%). *Anal.* Calc. for $C_{15}H_{22}N_2NiO_4$: C, 50.99; H, 6.23; N, 7.93. Found: C, 50.91; H, 6.17; N, 7.91%. UV–Vis–NIR (methanol, nm) λ_{max} = 609, 753, 900.

2.2.4. Synthesis of Complex [NiL^2(NCS)] (**2a**)

After adopting the same procedure as for **2**, aqueous solution of sodium thiocyanate (0.162 g, 2 mmol) was added. The solution turned reddish brown immediately from green. Final solution was kept for crystallisation. X ray suitable red crystals of complex **2a** were obtained from the resulting solution after 2 days. (Yield 82%). *Anal.* Calc. for $C_{14}H_{17}N_3NiOS$: C, 50.29.47; H, 5.08; N, 12.57. Found: C, 50.23; H, 5.06; N, 12.53%. UV–Vis–NIR (methanol, nm) λ_{max} = 473, 753, 873.

2.3. X-ray data collection and structure determination

Diffraction data for **1**–**4** were collected at room temperature (293 K) on a Bruker Smart CCD diffractometer equipped with graphite–monochromated Mo Kα radiation (k = 0.71073 Å). Cell refinement, indexing and scaling of the data set were carried out using Bruker SMART APEX and Bruker SAINT package [23]. The structure were solved by direct methods and subsequent Fourier analyses [24] and refined by the full-matrix least-squares method based on F^2 with all observed reflections using SIR-92 and SHELX-97 [25], software. For the complexes, all non-hydrogen atoms were refined with anisotropic thermal parameters and the hydrogen atoms were fixed at their respective positions riding on their carrier atoms and refined anisotropically. All the calculations were performed using the WinGX System, Ver 1.80.05 [26], PLATON99 [27], ORTEP3 [28] programs. Selected crystallographic data and refinement details are displayed in Table 1.

2.4. Computational details

Unrestricted calculations were carried out using the Gaussian09 package [29]. The hybrid density function method known as B3LYP was applied [30]. Effective core potentials (ECP) were used to represent the innermost electrons of the nickel and the basis set of valence double-ζ quality for associated with the pseudopotentials known as LANL2DZ [31]. The basis set for the main group elements was 6-31G* (S, C, N, O and H) [32]. Solvent effects of methanol and water were taken into account by PCM calculations [33], keeping the geometry optimized for gas phase (single-point calculations).

2.5. Bio-activity

2.5.1. Isolation and culture of Erhlich's ascities carcinoma (EAC) cells

EAC cells were isolated aseptically from the peritoneal cavity of tumor-bearing mouse after injecting 2–3 ml of PBS into the peritoneal cavity. The collected cells were placed in sterile petriplates and incubated at 37 °C for 2 h to separate the tumor cells from cells of macrophage lineage. The non-adherent tumor cells were

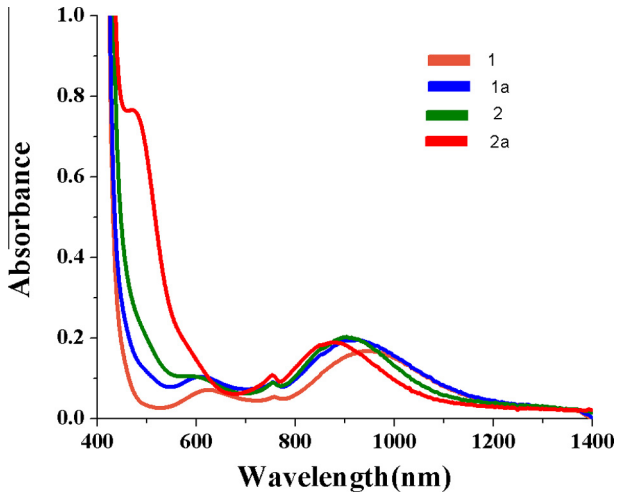

Fig. 1. UV–Vis spectra of 10^{-2} (M) solution of complex **1**, **1a**, **2**, **2a** in methanol medium.

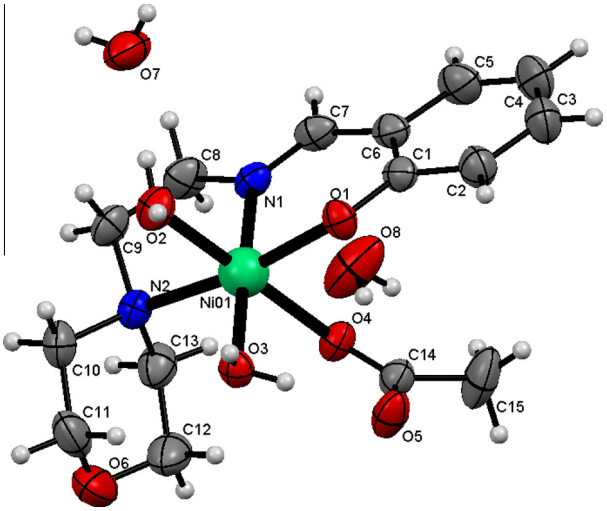

Fig. 2. Molecular structure of complex **1** with the atom numbering scheme.

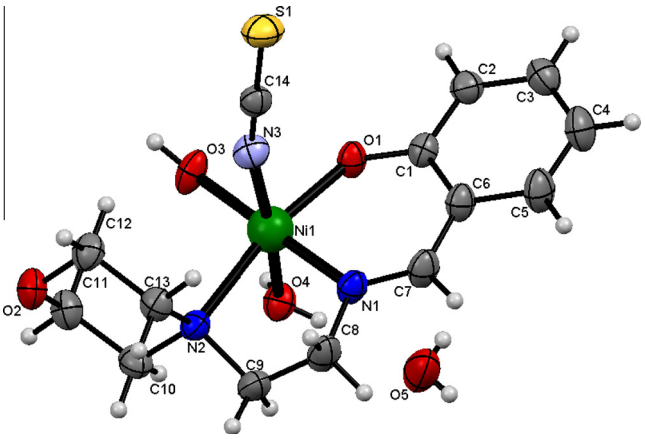

Fig. 3. Molecular structure of complex **1a** with the atom numbering scheme.

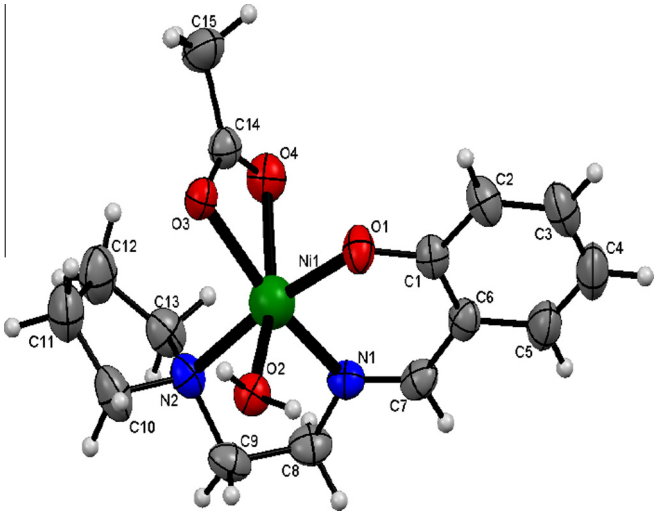

Fig. 4. Molecular structure of complex **2** with the atom numbering scheme.

aspirated out gently and washed repeatedly with PBS and then cultured in RPMI-1640 medium in presence of 10% FBS, Streptomycin (100 U/ml) and gentamycin (50 U/ml) at 37 °C in a CO_2 incubator.

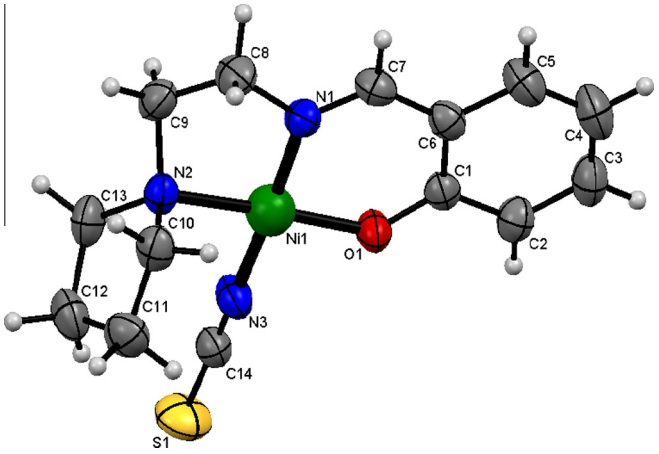

Fig. 5. Molecular structure of complex **2a** with the atom numbering scheme.

The cells were serum-starved for 24 h. After 24 h the cells were cultured with increasing doses (0–150 μM) of the compounds (**1**–**4**) and also in presence of a standard free radical scavenger 10 nM N-acetyl cysteine (NAC). At the end of the culture, media along with the cells were aspirated and were aspirated and were centrifuged at 3000 rpm for 5 min. The cells from each group were collected and with them different experiments were performed [34,35].

2.5.2. Isolation and culture of hepatocytes

Liver was perfused *in situ* with collagenase (0.05% p/v) and then the liver was removed. A portion of the liver was chopped with a blunt forceps and single cell suspensions were made in RPMI-1640. The cell population was passed through a nylon mesh with 70 μM pore size. Cell viability was determined using Trypan blue exclusion test and then the cells were cultured in the same way the EAC cells were cultured [35,36].

2.5.3. Cytotoxicity assay

Change in percentage of viability of EAC cells and hepatocytes after treating them with the increasing doses of the compounds was determined by the 3-(4,5-dimethylthiazol-2-yl)-2,5-diphenyl te-trazolium bromide (MTT) assay. The cultured cells were resuspended in PBS containing MTT (0.05 mg/ml) and were incubated for 4 h at 37 °C. The media containing MTT was aspirated out and 200 μl of dimethyl sulfoxide was added to dissolve the formed insoluble formazan salt. The absorbance was read spectrophotometrically at 540 nm and the number of viable cells is proportional to the amount of formazan salt formed and was measured as the percent of the control [37].

2.5.4. Detection of intracellular ROS content

EAC cells, after treatment with the compounds, were lysed in ice-cold lysis buffer (50 mM Tris–HCl, 150 mM NaCl, 1 mM EGTA, 1 mM EDTA, 20 mM NaF, 100 mM Na_3VO_4, 0.5% NP-40, 1% Triton X-100, 1 mM PMSF, pH 7.4) with freshly added protease inhibitor cocktail. It was centrifuged at 14,000*g* for 25 min at 4 °C and the supernatant (total cell lysate) was collected, aliquoted and was used for estimation of intracellular ROS content. The protein content in the lysates was measured by Micro Lowry method for estimation of protein. ROS content of the EAC cells was measured according to Toban-Velasco et al. [40]. 5 μl of whole cell lysate of each group were incubated in presence of 5 mM dihyroethidium at 37 °C for 60 min. Fluorescent signals were recorded at the end of the incubation at an excitation wavelength of 480 nm and an emission wavelength of 525 nm in a spectrofluorimeter (JASCO).

Table 2
Selected bond distances for complexes **1**–**2a**.

1		1a		2		2a	
Ni01–O1	2.0377(15)	Ni1–O1	2.0351(11)	Ni1–O1	2.0187(17)	Ni1–O1	1.8343(18)
Ni01–O2	2.110(2)	Ni1–O3	2.0544(11)	Ni1–O2	2.0908(16)	Ni1–N1	1.8450(19)
Ni01–O3	2.0384(18)	Ni1–O4	2.1711(12)	Ni1–O3	2.1142(16)	Ni1–N2	1.959(2)
Ni01–O4	2.1182(15)	Ni1–N1	2.0056(11)	Ni1–O4	2.1633(19)	Ni1–N3	1.863(2)
Ni01–N1	2.0024(18)	Ni1–N2	2.2771(12)	Ni1–N1	1.999(2)		
Ni01–N2	2.2307(17)	Ni1–N3	2.0486(14)	Ni1–N2	2.1843(19)		

Table 3
Selected bond distances for complexes **1–2a**.

1		1a		2		2a	
O1–Ni01–O2	90.18(7)	O1–Ni1–O3	87.14(5)	O1–Ni1–N2	172.21(7)	O1–Ni1–N1	94.71(7)
O1–Ni01–O3	90.68(7)	O1–Ni1–O4	87.72(4)	O1–Ni1–N1	90.13(7)	O1–Ni1–N2	176.37(7)
O1–Ni01–O4	86.58(6)	O1–Ni1–N1	90.75(5)	O2–Ni1–O3	97.28(7)	O1–Ni1–N3	86.44(8)
O1–Ni01–N1	89.77(7)	O1–Ni1–N2	169.30(4)	O2–Ni1–O4	158.95(7)	N1–Ni1–N2	85.70(8)
O1–Ni01–N2	170.83(6)	O1–Ni1–N3	91.72(5)	O2–Ni1–N1	95.30(7)	N1–Ni1–N3	175.41(8)
O2–Ni01–O3	87.05(7)	O3–Ni1–O4	82.51(5)	O2–Ni1–N2	87.40(7)	N2–Ni1–N3	93.43(8)
O2–Ni01–O4	174.38(7)	O3–Ni1–N1	176.13(4)	O2–Ni1–C14	128.20(7)		
O2–Ni01–N1	94.80(8)	O3–Ni1–N2	99.88(5)	O3–Ni1–O4	61.71(7)		
O2–Ni01–N2	86.67(7)	O3–Ni1–N3	89.46(5)	O3–Ni1–N1	167.31(7)		
O3–Ni01–O4	88.40(6)	O4–Ni1–N1	94.17(5)	O3–Ni1–N2	99.10(7)		
O3–Ni01–N1	178.10(7)	O4–Ni1–N2	85.21(4)	O3–Ni1–C14	31.13(6)		
O3–Ni01–N2	97.75(7)	O4–Ni1–N3	171.97(5)	O4–Ni1–N1	105.67(7)		
O4–Ni01–N1	89.78(7)	N1–Ni1–N2	81.77(5)	O4–Ni1–N2	96.79(7)		
O4–Ni01–N2	97.22(6)	N1–Ni1–N3	93.85(5	O4–Ni1–C14	30.75(7)		
N1–Ni01–N2	81.93(7)	N2–Ni1–N3	96.39(5)	N1–Ni1–N2	83.19(7)		
				N1 -Ni1 –C14	136.19(7)		
				N2 –Ni1 -C14	101.60(7)		

A standard curve was prepared using increasing concentration of DHE incubated in parallel and results were expressed as moles of DHE produced per mg of protein [38–40].

2.5.5. Detection of DNA fragmentation by fluorescence microscopy

For detection of DNA fragmentation, which is hallmark of apoptosis, in EAC cells treated with or without increasing doses of the compounds, the EAC cells were fixed and nuclear DNA stained with DAPI (0.2 mg/ml for 15 min at room temperature). A fluorescent microscope was used to detect the signal from DAPI. Digital images were captured and were controlled with Dewinter Caliper Pro software [34].

2.5.6. DNA binding studies of the compounds by competitive fluorescence displacement assay

Interactions of the prepared compounds with double stranded DNA were studied by incubating the DNA–ethidium bromide complex with the complexes and the decrease in fluorescence was measured. 3.9 μM DNA (genomic DNA isolated from EAC cells using the method of Laird et al., 1991) was incubated with 1.1 μM ethidium bromide and various concentrations of the complexes. The reaction mixtures were excited at 552 nm and the fluorescence intensities were recorded at 624 nm using a JASCO spectroflourimeter [20,41].

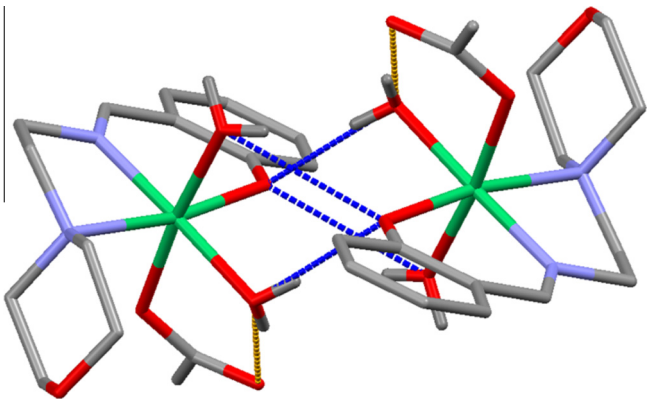

Fig. 6. Intermolecular H-bonding (blue dots) and intramolecular H-bonding (yellow dots) present in **1**. (Color online.)

3. Result and discussion

3.1. Syntheses, FT-IR spectra and UV–Vis spectra of the complexes

Two Schiff base ligands HL^1 and HL^2 are prepared through the classical method where salicylaldehyde is refluxed with N-(2-aminoethyl)-morpholine and N-(2-aminoethyl)-pyrrolidine, respectively in methanol medium for half an hour. HL^1 and HL^2 are further treated with nickel(II) acetate *in situ* separately to prepare complexes **1** and **2** respectively. Whereas, separate treatment of HL^1 and HL^2 with nickel(II) acetate and followed by sodium thiocyanate give complexes **1a** and **2a** respectively. All the four complexes are characterized by routine physicochemical techniques as well as by X-ray single crystal structure analyses. All the complexes show IR bands due to C=N stretch in the range 1618–1649 cm^{-1} and skeleton vibrations in the range 1536–1560 cm^{-1}. **1a** and **2a** have one sharp peak around 2100 cm^{-1} is due to C=N stretching of SCN ligand. A broad band in the range 3300–3500 cm^{-1} is due to hydrogen bonded O–H group of coordinated water molecule present in complexes **1**, **1a** and **2**. (Supporting Information, Figs. S1–S4). But such peak is absent in case of **2a** which implies the absence of hydrogen bonded O–H group. Magnetic susceptibility measurements for **1**, **1a** and **2** ($\mu_{eff} \approx 3.2$ B.M. at 298 K) suggest that nickel(II) possesses octahedral configuration whereas diamagnetic **2a** nickel(II) acquire square planar geometry. Electronic spectra (Fig. 1) recorded in methanol also reveal that coordination environment around nickel(II) in **1**, **1a**

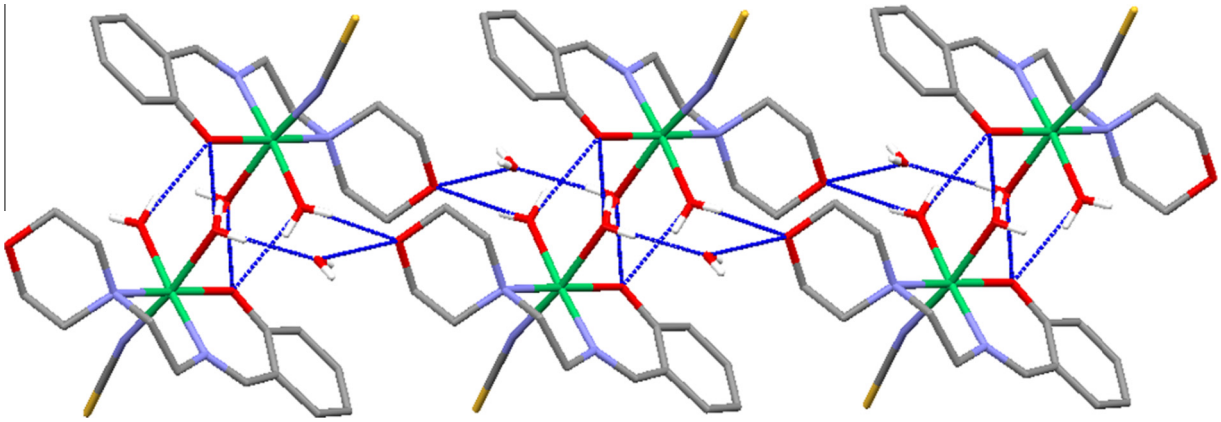

Fig. 7. H-bonded (blue dots) polymeric structure of **1a**. (Color online.)

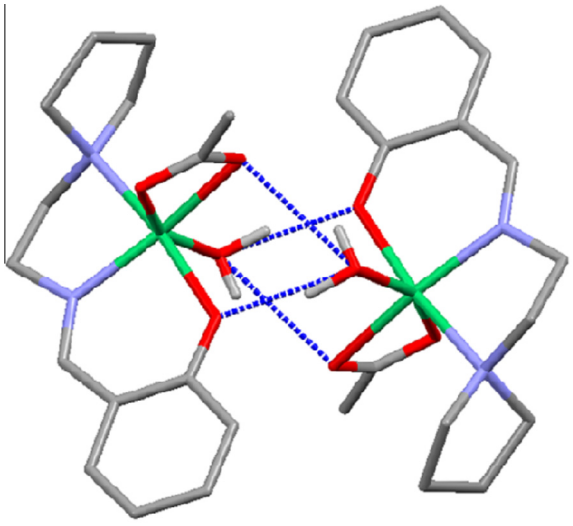

Fig. 8. Dimerization of complex **2** via intermolecular H-bonding (blue dotts). (Color online.)

and **2** is roughly octahedral and square planar in **2a** [42,43]. Complex **1**, **1a**, **2** display three weak absorption bands at ~615, ~755 and ~900 nm (ε/dm^3 mol^{-1} cm^{-1}, 3–10) assigned to spin-allowed $^3A_{2g} \rightarrow {}^3T_{1g}(P)$, $^3A_{2g} \rightarrow {}^3T_{1g}(F)$ and $^3A_{2g} \rightarrow {}^3T_{2g}(F)$ transitions respectively expected for octahedral d^8 ions. In case of complex **2a**, bands around ~755 and ~920 are slightly blue shifted. Disappearance of peak around ~615 nm along with the generation of one new intense bands for **2a** at the lower wavelength region [~471 nm (ε/dm^3 mol^{-1} cm^{-1})] indicates a large crystal-field splitting and is consistent with the square planar geometry of nickel(II) as reported previously [44].

3.2. Crysallographic description of complexes *1–4*

The structure of complexes have been depicted in Figs. 2–5. All the four complexes are discrete mononuclear in nature. Complex **1** & **2** are made using tridentate ligand HL^1 whereas **3** & **4** are made with another tridentate ligand HL^2. Both the ligands have N, N, O donor site, where HL^1 and HL^2 contain morpholine and pyrrolidine moiety respectively. Complexes **1**, **1a** and **2** have one octahedrally disordered Ni^{II} centre. On the other hand in complex **2a**, Ni^{II} centre have perfectly square planar geometry. Complex **1** contains two coordinating water molecules (one in axial and another in equatorial position with respect to ligand plane) and one acetate anion (present in axial position). Here acetate anion is bridged via mono dentate mode. In **1a**, Ni^{II} is coordinated via three donor sites of HL^1, N of one isothicyanato ligand and two water molecules. In complex **2**, one acetate anion coordinate Ni centre through two oxygen atoms in bidentate fashion. Sixth position is occupied by one metal coordinated water molecule. Complex **2a**, Ni^{II} is coordinated via three donor site of HL^2 and Nitrogen of one isothicyanato ligand. Selected bond lengths are reported in Table 2. The Ni–N1, Ni–N2, Ni–O1 bond distances vary in the ranges 1.8450(19)–2.0056(11), 1.959(2) –2.2307(17), and 1.8343(18)–2.0377(15) Å, respectively. Selected bond angles are shown in Table 3. The mean N1–Ni–O1, N1–Ni–N2, and O1–Ni–N2 bond angles are 91.34°, 83.15°, and 172.18°, respectively. Packing diagram for all the complexes are shown in Fig. S5–S8 (See Supporting Information). The adjacent mononuclear molecules of **1** are linked by O–H(water) $\cdots$O(phenoxyl) intermolecular hydrogen bonds. Each molecule of **1** has an intramolecular hydrogen bond O–H(water)$\cdots$O(acetate) also as depicted in Fig. 6. Hydrogen bonded 1D polymeric structure of **1a** is represented in Fig. 7. Dimerization of single molecule of **2** via hydrogen bonding has been illustrated in Fig. 8.

3.3. DFT Study

In an attempt to understand the formation of nickel complexes, we have performed a theoretical study based in DFT calculations to evaluate the thermodynamic feasibility of these compounds. In addition to the energetic profile and relative stability of the species involved, our study provides an insight into structural features of involved complexes. In our calculation, solvent effects have been considered in all reactions by an implicit method to obtain Gibbs free energies. Both methanol and water are taken as solvent, but only former will be discussed in this section. We have defined two main pathways in our study: (*a*) substitution of the monodentate acetate by a isothiocyanate one, via a pentacoordinated intermediate; and, (*b*) acetate isomerization to bidentate coordination mode replacing a water molecule, following by the introduction of a isothiocyanate to exchange it, generating a square planar complex. In all cases, the pathways are evaluated from the octahedral compound $[Ni(\kappa^1\text{-}O_{Ac})(H_2O)_2(L)]$ (**A**), having L an *O,N,N′*-tridentate ligand.

3.3.1. Substitution of an octahedral complex

Since the most favored reaction for ligands substitution of hexacoordinated complexes proceed via a pentacoordinated intermediates in two steps, this pathway is studied (Scheme 2). The pentacoordinated intermediates (**AB**) have been characterized for both L^{Morph} and L^{Pyrr} ligands, having similar stability from the

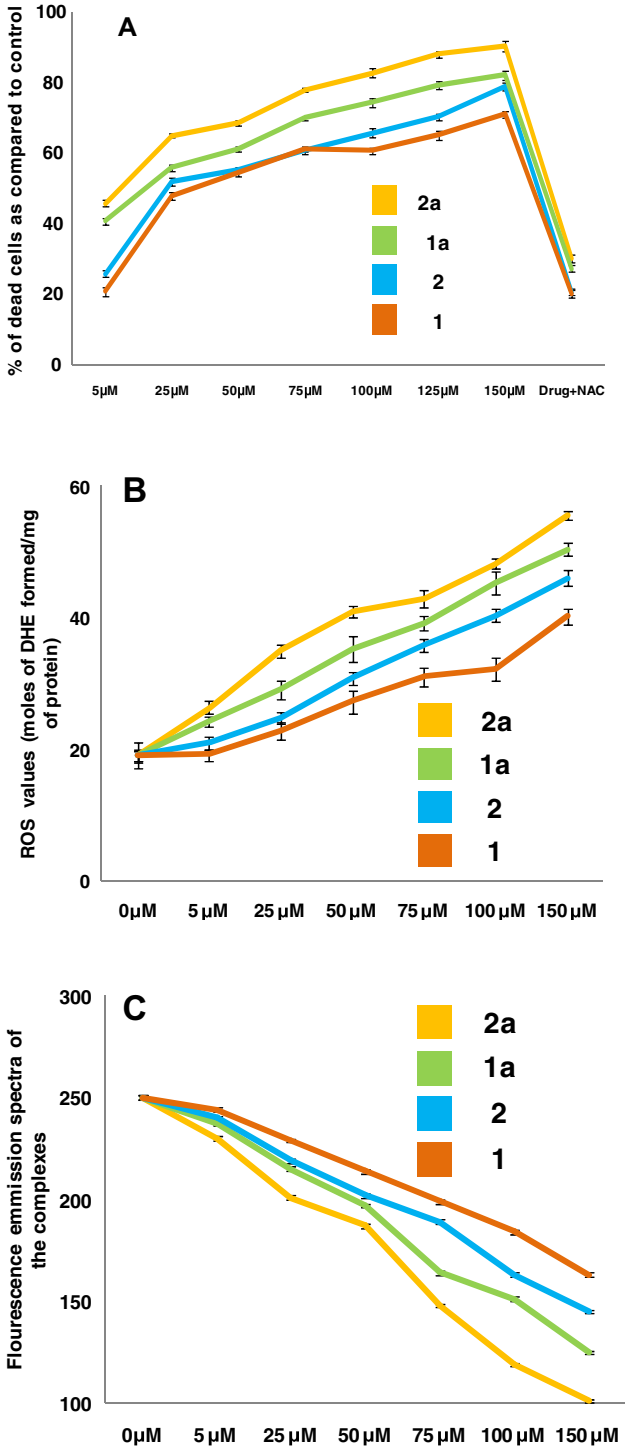

Fig. 9. Effect of the complexes **1**, **1a**, **2** and **2a** on tumor cell survival. EAC cells were incubated with increasing doses of the complexes (0–150 μM) in presence of 10 mM N-acetyl cysteine (NAC) for 24 h. After 24 h, cells were collected and assayed for the effect of the compounds on: (A) Cell death – For determination of cell death, harvested cells were incubated with MTT for 4 h and the amount of formation of formazan salt was measured at 540 nm using a spectrophotometer. (B) Intracellular ROS content was estimated by incubating the cell lysates from each groups with DHE (25 μg/ml) for 1 h using a spectrophotometer using excitation and emission wavelengths of 495 nm and 525 nm respectively. (C) DNA fragmentation – For detection of DNA fragmentation, treated EAC cells were fixed, permeabilised and stained with DAPI and visualized under a fluorescence microscope. The figures shown here are representative of six different figures with similar results. All values represent mean ± S.E. of six independent experiments in each case.

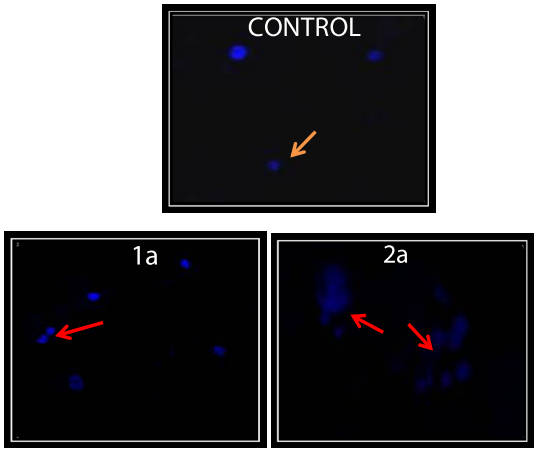

Fig. 10. Fluorescence emission spectra of EB–DNA fragmentation in absence (Control) and presence of complex **1a** and **2a**.

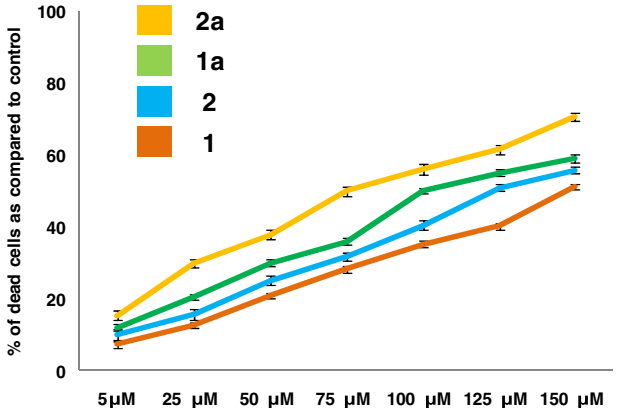

Fig. 11. Effect of the complexes on survival of normal primary mouse hepatocytes. Isolated hepatic cells were incubated with increasing doses of the complexes (0–150 μM) for 24 h. After 24 h, cells were collected and the percentage of dead cells was assayed. For determination of cell death, harvested cells were incubated with MTT for 4 h and the amount of formation of formazan salt was measured at 540 nm using a spectrophotometer.

reactants, about 28 kcal/mol. Besides the charges of reactants and products are not the same, the high ability of acetate and isothiocyanate to generate hydrogen bonds will affect dramatically on the thermodynamics. As example, when one solvent molecule is explicitly included by forming a hydrogen bonding, they are stabilized only 4 kcal/mol from insolated models. Nevertheless, we have decided to generate pentacoordinated intermediates by lengthening of sixth ligand and full reoptimizaton of molecular structure. When distances are sufficiently large to not find energetic changes, similar energy from the reactants about 15 kcal/mol has been obtained. And now, the final substituted octahedral complex (**B**) is only +5 kcal/mol from the reactants. Moreover, the influence of solvent, methanol or water, is very scarce in this pathway, and all energetic differences are less than 1 kcal/mol.

All three involved complexes present same structural trends. Hexacoordinate complexes presents particularly identical distances for three donors (O_{Ar},N_{Im},N_{Am}) arount the nickel, Ni–$O_{Ar} \approx 2.04$, Ni–$N_{Im} \approx 2.01$, but small diferences of 0.03 Å are found for Ni–N_{Am}, being larger for L^{Morph} than L^{Pyrr} complexes (2.23 and 2.20 Å, respectively). The *fac* disposition of tridentate ligand is completed by one water in equatorial, which Ni–O_{Eq} distances (2.11 and 2.22 Å in **A** and **B**, respectively) change by the presence of intramolecular hydrogen bonding in acetate complexes but

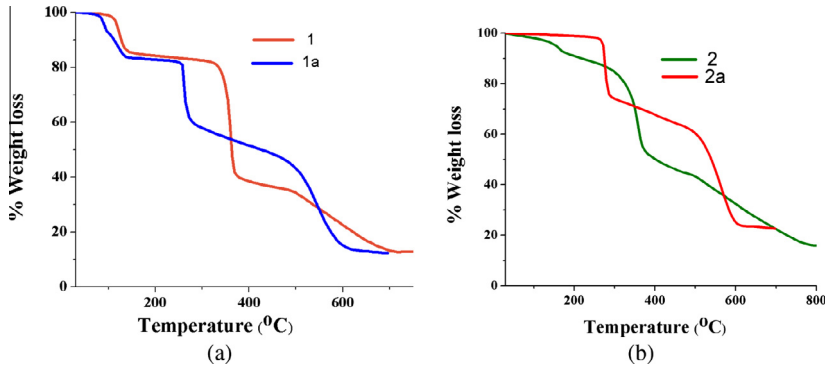

Fig. 12. TGA plot of complex (a) **1** and **1a**; (b) **2** and **2a**.

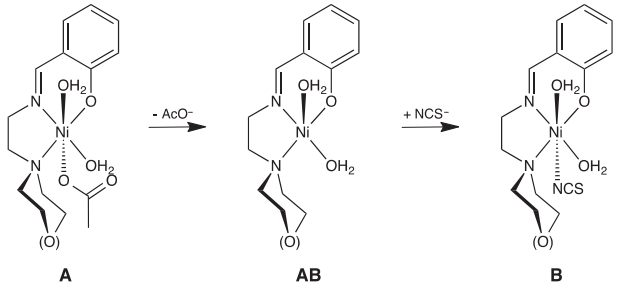

Scheme 2. Substitution of acetate ligand by isothiocyanate in an octahedral complex.

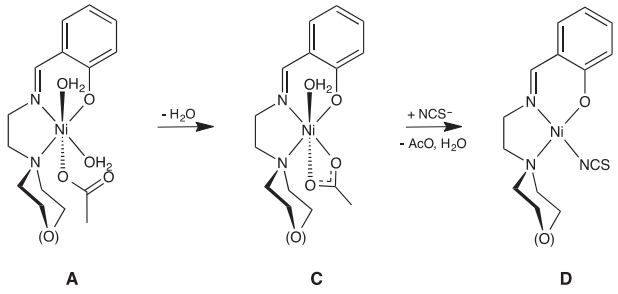

Scheme 3. Genaration of square planar complex from octahedral one.

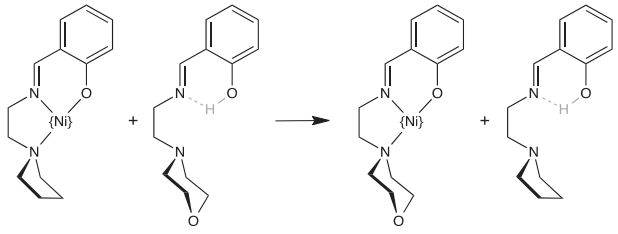

Scheme 4. Interchanging of two lignads.

absence in thiocyanate one. The axial positions with leaving ligands are identical depending of the nature of this ligand (Ni–O_{Ac}/N_{NCS} are 2.04 and 2.08 Å), and we would remark the angular geometry of coordinated *N*-thiocyanate (121°). Finally, small changes are found for axial water molecule induced by *trans* influence (2.29 and 2.26 Å in **A** and **B**, respectively).

The pentacoordinated species (**AB**) are clearly decribed as square pyramidal, having distances shorter than those found in hexacoordinate complexes. The three donors (O_{Ar},N_{Im},N_{Am}) of

Table 4
Half maximal inhibitory concentration (IC_{50}) in μM of the complex.

Complex	Half maximal inhibitory concentration (IC_{50}) in μM on tumor cells
2a	19.634
1a	22.32
2	24.08
1	26.08
cis-Platin	24.1

Table 5
Half maximal inhibitory concentration (IC_{50}) in μM of the complex towards normal cell.

Complex	Half maximal inhibitory concentration (IC_{50}) in μM on primary mouse hepatocytes
2a	41.96
1a	61.39
2	79.92
1	98.42
cis-Platin	24.1

tridentate ligand are situated into basal plane. The distances Ni–O_{Ar} and Ni–N_{Im} are 1.93 and 1.98 Å, and differences of 0.02 Å for Ni–N_{Am} are newly found in L^{Morph} (2.13) and L^{Pyrr} (2.11) complexes. The environment is completed with two water molecules in the fourth basal and the aplical positions at 2.16 and 2.11 Å, respectively, and other structural changes are less important.

Another interesting point for these nickel compounds are its electronic structure. Since nickel(II) is a d^8 ion, it should present two unpaired electrons in pseudo-octahedral or square-pyramidal environments. Our calculations show spin densities in the metal atoms between 1.58 and 1.63, revealing that 80% of those two electrons are locating in the nickel atom. More than 10% are delocalized in the tridentate ligand, specially in the aromatic and iminic framework. Additionally, frequency calculations display characteristics in the infrared spectra: one band about 1633 cm^{-1} for terminal carbonyl group in acetate complex (**A**), and two about 2107 and 811 cm^{-1} for thiocynate one (**B**). An imine stretching band changes from 1710 (**A**) to 1707 (**B**) cm^{-1}.

3.3.2. Generating a square-planar complex

A second pathway to obtain a thiocyanate complex from acetate one was studied. It proceeds from [Ni(κ^1-O_{Ac})(H_2O)$_2$(L)] complex (**A**) that isomerizes to [Ni(κ^2-O_{Ac})(H_2O)(L)] (**C**) changing the coordination mode for acetate ligand, and after thiocyanoate replaces the carboxylato generating a square-planar complex D (Scheme 2). The first step corresponds to an isomerization of the acetate anion in triplet as ground state for the complex (and ~80% of the spin densities

remains in nickel atoms). Our calculations reveal that chelate complex (**C**) is only 0.8 (L^{Morph}) and 1.1 (L^{Pyrr}) kcal/mol higher in energy than monodentate one, but they become the more stable if the leaving water molecules remain bound to coordinated water, as it is found in crystal structures (-2.4 ans −1.7 kcal/mol for L^{Morph} and L^{Pyrr} derivatives, respectively). Moreover, an accessible transition state for this isomerization are localizated having low energy for the two systems (∼+7 kcal/mol). For this reason, we can propose an easy accessibility to the interconversion between coordination modes of acetate ligand.

Optimized geometries (**C**) reveal minor changes in the distances between nickel and tridentate ligand, in comparison with related terminal complexes (**A**), whereas Ni–O distances are about 2.10 and 2.12 Å for equatorial and axial bonds, larger than monodentate one (2.04 Å). However, an important distortion about ideal octahedral geometry is observed by chelate requirements of four-membered rings. Carboxylate frequencies in the would appear at 1612 and 1488 cm^{-1} (**C**) according with the chelate mode (Δ = 124 cm^{-1}), and they pattern are similar to those found monodentate complexes (**A**) due the intramolecular hydrogen bonding (Δ = 171 cm^{-1}). However, the imine stretching is moved to 1698 cm^{-1} (**C**).

The following step for the second path is the substitution of both acetate and water by thiocianate. This reaction leads a change in the spin ground state, generating a diamagnetic ion, induced by square-planar geometry around the nickel atoms, being null spin density and diamagnetic behavior. The evaluated energies for this reaction are unfavored by more than +18 kcal/mol. When water molecule is added to the leaving acetate generating hydrogen bondins, they decrease to +14 kcal/mol, being always L^{Pyrr} derivative more preferred than L^{Morph} one. All metal–ligand distances in the square-planar complexes (**D**) are dramatically shorter that those found in octahedral complexes (more than 0.1 Å). A special case is found for the Ni-NCS distance (1.88 *vs.* 2.08), probably by major contribution of the π-backbonding in the square planar geometry. The stereochemical modification of the nickel atom produces important changes in the infrared spectra: (*a*) the imine stretching decrease to 1682 cm^{-1}, (*b*) C-S band of thiocynate increase to 888 cm^{-1}, and (*c*) C–N band of thiocyanate is slight moved to 2117 and 2129 cm^{-1}, for L^{Morph} and L^{Pyrr} complexes, respectively.

3.3.3. Interchanging ligands

Finally, we have studied the interchanging reactions for nickel complexes, as it is shown in Scheme 3. In all cases, we have obatined that complexes containing L^{Pyrr} are more favored than L^{Morph} ones by 1.3–3.2 kcal/mol. It suggests than L^{Pyrr} acts as better ligand than L^{Morph}, according to largest Brönsted basicity of the pyrrolidine than the morpholine (pK_b are 2.7 and 5.5, respectively). In the neutral form of tridentate ligand (as phenol derivative), identical energies have been found in both metahnol and water solvents, indicating that it has not influence of the media. However, when uncoordinated ligand is considered in its anion form of (as phenolate salt), water stabilizes slightly L^{Pyrr} complexes than L^{Morph}, by only 0.3 kcal/mol. The theoretical data has been tabulated in Table S1–S3 (Supporting Information). (See Scheme 4)

3.4. Biological activity of the complexes

The effect of the treatment of the compounds on Erhlich's ascites carcinoma cells on cell survivality is determined by MTT assay. It is observed that among the four compounds, square planar **2a** is most efficient in killing the tumor cells and least cytotoxicity is observed when the cells are treated with **1**(Fig. 9A). In all the cases, cytotoxicity increased with increasing dose of the compounds and maximum cytotoxicity is observed at the highest dose i.e., 150 μM. Table 4 shows the IC_{50} values of complexes **2a**, **1a**, **2**, **1** and a standard chemotherapeutic drug *cis*-platin towards cancer cells. Our results strongly suggest that the Ni complexes especially **2a**, **1a** and **2** are effective than *cis*-platin on EAC cells.

To explore the nature of the cell death by compounds we investigate the level of ROS generation in the EAC cells. We have found that treatment of the EAC cells with the compounds increased ROS generation by more than 2fold. Researchers have established that cancer cells have higher basal level of ROS and any agent that increases ROS generation is termed chemotherapeutic agent (Manna et al., 2012) [45]. In the present study we have shown that our compounds increased the level of ROS in EAC cells which ultimately led to EAC cell death (Fig. 9B). To confirm that ROS is the main player in orchestrating EAC cell death, we co-treated the cells with a standard ROS scavenger N-acetyl cysteine (NAC). We found that co-treatment of the cells with 10 mM NAC protected the EAC cells from ROS induced cell death by the compounds as evidenced by increase in cell viability in the NAC co-treated groups (Fig. 9A).Induction of apoptosis by the compounds **2a** and **1a** are confirmed by observing DNA fragmentation (hallmark of apoptotic cell death) in the EAC cells following treatment of EAC cells by the compounds (Fig. 9C).

We have studied fluorescence quench of ethidium bromide bound DNA by the compounds as a function of interaction between the complexes and the DNA. Fig. 10 shows increasing concentration of four complexes results in decrease in fluorescence intensity of the ethidium–DNA complex. This indicates that all the four complexes are able to kick out ethidium bromide from DNA. Our data is in accordance with the reports of other investigators which states that Ni complexes exhibit groove binding interactions with DNA (Zhu et al., 2010)[20].

The most common problem with most chemotherapeutic drugs is that the drugs are toxic towards both cancer cells as well as normal cells. Our data shows that the Ni complexes are comparatively less toxic towards normal primary hepatocytes than EAC cells. The IC_{50} of the compounds towards hepatocytes is much higher when compared to IC_{50} of *cis*-platin. So it can be said that the complexes are highly toxic to cancer cells but less toxic towards normal cells (Fig. 11, Table 5).

3.5. Thermogravimetric analysis

Thermal studies of all the four complexes show stepwise decomposition. Fig. 12(a) and Fig. 12(b) depict the TGA diagrams of the complexes of ligands HL^1 and HL^2, respectively. Decomposition pattern clearly suggest that **2a** is the most stable among the four. **2a** starts to disintegrate over 250 °C whereas other complexes start to lose weight below 100 °C. That further tells **1**, **1a** and **2** contain water molecules in crystal structure but **2a** doesn't bear any water molecules. The loss of four water molecules present in complex **1** takes place in single steps whereas **1a** loss three water molecules in two successive steps on heating. First step weight loss for **1** and **1a** are 14.7% (Calcd. 17.07%) and 16.3% (Calcd 13.4%), receptively between 70 °C and 160 °C. Complex **2** shows first step weight loss of 7.5% (Calcd. 5.0%) corresponds to the elimination of one water molecules in the temperature range of 40–170 °C. All four species on further heating generate NiO as the thermally stable end product (for complex **1**, Expt. wt loss = 86.7% at 730 °C, theo. Wt. loss = 82.4%; for complex **1a** Expt. wt loss = 86.5% at 640 °C, theo. Wt. loss = 81.6%; for complex **2** Expt. wt loss = 83.23% at 800 °C, theo. Wt. loss = 78.9% and for complex **2a** Expt. wt loss = 76.4% at 630 °C, theo. Wt. loss = 77.6%).

4. Conclusions

Two N,N,O-donor Schiff-base ligands namely 2-[(2-Morpholin-4-yl-ethylimino)-methyl]-phenol and 2-[(2-Pyrrolidin-1-yl-ethylimino)-methyl]-phenol have been designed and synthesized with the view to explore the influence of non-coordinating heterocyclic parts of the ligands on the structural variation of nickel complexes in presence of acetate and isothiocyanate as co-ligands. In presence of acetate as co-ligand, both Schiff-base ligands yield octahedral complexes, whereas, isothiocyanate helps to generate nickel complexes with two different configurations, octahedral with HL^1 and square-planar with HL^2. Investigation reveals that the nature of the heterocyclic ring part present in N,N,O donor Schiff-bases i.e. "morpholin" moiety in ligand HL^1 and "pyrrolidine" moiety in ligand HL^2 is likely to be instrumental in generating Ni(II) complexes having different configuration in presence of SCN as co-ligand. DFT calculations optimized correctly the molecular geometries of involved species. However, relative energies of final isothiocyanoate complexes do not agree with obtained compounds. The presence of the intramolecular hydrogen bonding interactions modifies relative stability of calculated species, indicating that not only dielectric continuum has to be taken into account, and these interactions with protic solvents should be considered. Anticancer activity of the complexes on Erhlich's ascities carcinoma (EAC) reveals that Ni(II) having square-planar geometry exhibits better activity over analogous Ni(II) complex with octahedral geometry.

Acknowledgements

We are thankful to University Grants Commission (UGC), New Delhi, India, for the Senior Research Fellowship to J.A [UGC/197/Jr. Fellow (enhancement) dated 26.02.2013]. G. A is also thankful to *Spanish Dirección General de Investigación* (DGI) through Grant CTQ2011-23862-C02 for financial support for this work. Allocation of computer facilities at IQTCUB is also acknowledged by G.A.

Appendix A. Supplementary data

CCDC 971485–971488 contains the supplementary crystallographic data for the four complexes. These data can be obtained free of charge via http://www.ccdc.cam.ac.uk/conts/retrieving.html, or from the Cambridge Crystallographic Data Centre, 12 Union Road, Cambridge CB2 1EZ, UK; fax: (+44) 1223 336 033; or e-mail: deposit@ccdc.cam.ac.uk. Supplementary data associated with this article can be found, in the online version, at http://dx.doi.org/10.1016/j.poly.2015.07.055.

References

[1] E. Ferentinos, D. Maganas, C.P. Raptopoulou, A. Terzis, V. Psycharis, N. Robertson, P. Kyritsis, Dalton Trans. 40 (2011) 169.
[2] D. Maganas, A. Grigoropoulos, S.S. Staniland, S.D. Chatziefthimiou, A. Harrison, N. Robertson, P. Kyritsis, F. Neese, Inorg. Chem. 49 (2010) 5079.
[3] J. Li, H. Song, C. Cui, J.-P. Cheng, Inorg. Chem. 47 (2008) 3468.
[4] O. Rotthaus, F. Thomas, O. Jarjayes, C.P.E. Saint-Aman, J.-L. Pierre, Eur. J. Inorg. Chem. 12 (2006) 6953.
[5] S. Mukhopadhyay, D. Mandal, D. Ghosh, I. Goldberg, M. Chaudhury, Inorg. Chem. 42 (2003) 8439.
[6] D. Das, N. Ray Chaudhuri, A. Ghosh, Polyhedron 15 (1996) 3919.
[7] J. Adhikary, P. Chakraborty, T. Chattopadhyay, R. Prasad, Y. Motro, B. Koch, F.A. Mautner, Y. Miller, D. Das, Polyhedron 93 (2015) 55.
[8] F. Meyer, H. Kozlowski, Comprehensive Coordination Chemistry II: From Biology to Nanotechnology, in: J.A. McCleverty, T.J. Meyer (Eds.), 6, Elsevier, Oxford, 2004, p. 247.
[9] D. Nakane, Shin-ich Kuwasako, M. Tsuge, M. Kubo, Y. Funahashi, T. Ozawa, T. Ogurab, H. Masuda, Chem. Commun. 46 (2010) 2142.
[10] D. Nakane, Y.W. Tsutsui, Y. Funahashi, T. Hatanaka, T. Ozawa, H. Masuda, Inorg. Chem. 53 (2014) 6512.
[11] Y.Y. Yu, H.D. Xian, J.F. Liu, G.L. Zhao, Molecules 14 (2009) 1747.
[12] P.G. Cozzi, Chem. Soc. Rev. 33 (2004) 410.
[13] G.B. Bagihalli, S.A. Patil, P.S. Badami, J. Enzyme Inhib. Med. Chem. 24 (2009) 730.
[14] M.M. Omar, G.G. Mohamed, A.A. Ibrahim, Mol. Biomol. Spectrosc. 73 (2009) 358.
[15] S.S. Matkar, L.A. Wrischnik, P.R. Jones, U. Hellmann-Blumberg, Biochem. Biophys. Res. Commun. 343 (2006) 754.
[16] O. Kornyushyna, A.J. Stemmler, D.M. Graybosch, I. Bergenthal, C.J. Burrows, Bioconjugate Chem. 16 (2005) 178.
[17] E. Moldrheim, M.J. Hannon, I. Meistermann, A. Rodger, E. Sletten, J. Biol. Inorg. Chem. 7 (2002) 770.
[18] L.J. Childs, J. Malina, B.E. Rolfsnes, M. Pascu, M.J. Prieto, M.J. Broome, P.M. Rodger, E. Sletten, V. Moreno, A. Rodger, M.J. Hannon, Chem. Eur. J. 12 (2006) 4919.
[19] (a) J. Adhikary, P. Chakraborty, S. Das, T. Chattopadhyay, A. Bauzá, S.K. Chattopadhyay, B. Ghosh, F.A. Mautner, A. Frontera, D. Das, Inorg. Chem. 52 (2013) 13442;
(b) T. Chattopadhyay, M. Mukherjee, A. Mondal, P. Maiti, A. Banerjee, K.S. Banu, S. Bhattacharya, B. Roy, D.J. Chattopadhyay, T.K. Mondal, M. Nethaji, E. Zangrando, D. Das, Inorg. Chem. 49 (2010) 3121;
(c) T. Ghosh, J. Adhikary, P. Chakraborty, P.K. Sukul, M.S. Jana, T.K. Mondal, E. Zangrando, D. Das, Dalton Trans. 43 (2014) 841;
(d) A. Banerjee, A. Guha, P. Maiti, S. Goswami, T. Chattopadhyay, T.K. Mondal, S. Bhattacharya, E. Zangrando, D. Das, Transition Met. Chem. 36 (2011) 829.
[20] Li Na Zhu, De Ming Kong, X.Z. Li, G. Yu Wang, J. Wang, Y.W. Jin, Polyhedron 29 (2010) 574.
[21] D.M. Kong, J. Wang, L.N. Zhu, Y.W. Jin, X.Z. Li, H.X. Shen, H.F. Mi, J. Inorg. Biochem. 102 (2008) 824.
[22] R. Prabhakaran, P. Kalaivani, P. Poornima, F. Dallemer, G. Paramaguru, V.V. Padma, R. Renganathan, R. Huang, K. Natarajan, Dalton Trans. 41 (2012) 9323.
[23] Bruker, SMART, SAINT. Software Reference Manual Bruker AXS Inc., Madison, Wisconsin, USA, 2000.
[24] G.M. Sheldrick, Acta. Crystallogr. Sect. A 64 (2008) 112.
[25] G.M. Sheldrick, SHELXL 97, Program for the Refinement of Crystal Structures, University of Gottingen, Germany, 1997.
[26] L.J. Farrugia, J. Appl. Crystallogr. 32 (1999) 837.
[27] A.L. Spek, PLATON, Molecular Geometry Program, University of Utrecht, The Netherlands, 1999.
[28] L.J. Farrugia, J. Appl. Crystallogr. 30 (1997) 565.
[29] M.J. Frisch, G.W. Trucks, H.B. Schlegel, G.E. Scuseria, M.A. Robb, J.R. Cheeseman, G. Scalmani, V. Barone, B. Mennucci, G.A. Petersson, H. Nakatsuji, M. Caricato, X. Li, H.P. Hratchian, A.F. Izmaylov, J. Bloino, G. Zheng, J.L. Sonnenberg, M. Hada, M. Ehara, K. Toyota, R. Fukuda, J. Hasegawa, M. Ishida, T. Nakajima, Y. Honda, O. Kitao, H. Nakai, T. Vreven, J.A. Montgomery Jr., J.E. Peralta, F. Ogliaro, M. Bearpark, J.J. Heyd, E. Brothers, K.N. Kudin, V.N. Staroverov, T. Keith, R. Kobayashi, J. Normand, K. Raghavachari, A. Rendell, J.C. Burant, S.S. Iyengar, J. Tomasi, M. Cossi, N. Rega, J.M. Millam, M. Klene, J.E. Knox, J.B. Cross, V. Bakken, C. Adamo, J. Jaramillo, R. Gomperts, R.E. Stratmann, O. Yazyev, A.J. Austin, R. Cammi, C. Pomelli, J.W. Ochterski, R.L. Martin, K. Morokuma, V.G. Zakrzewski, G.A. Voth, P. Salvador, J.J. Dannenberg, S. Dapprich, A.D. Daniels, O. Farkas, J.B. Foresman, J.V. Ortiz, J. Cioslowski, D.J. Fox, Gaussian 09 (Revission B.1), Gaussian Inc., Wallingford CT, 2010.
[30] (a) A.D. Becke, J. Chem. Phys. 98 (1993) 5648;
(b) C. Lee, W. Yang, R.G. Parr, Phys. Rev. B 37 (1988) 785.
[31] P.J. Hay, W.R. Wadt, J. Chem. Phys. 82 (1985) 299.
[32] (a) P.C. Hariharan, J.A. Pople, Theoret. Chim. Acta 28 (1973) 213;
(b) M.M. Francl, W.J. Petro, W.J. Hehre, J.S. Binkley, M.S. Gordon, D.J. DeFrees, J.A. Pople, J. Chem. Phys. 77 (1982) 3654.
[33] (a) J. Tomasi, M. Persico, Chem. Rev. 94 (1994) 2027;
(b) C. Amovilla, V. Barone, R. Cammi, E. Cancès, M. Cossi, B. Mennucci, C.S. Pomelli, J. Tomasi, Adv. Quantum Chem. 32 (1998) 227.
[34] A. Bhattacharyya, T. Choudhuri, S. Pal, S. Chattopadhyay, G.K. Datta, T. Das, Carcinogenesis 24 (2003) 75.
[35] S. Mukherjee, S. Ghosh, S. Choudhury, A. Adhikary, K. Manna, S. Dey, J. Nutr. Biochem. 24 (2013) 2040.
[36] K. Manna, A. Khan, D.K. Das, S.B. Kesh, U. Das, S. Ghosh, J. Enthnopharmacol. 155 (2014) 132.
[37] T. Mosmann, J. Immunol. Methods 65 (1983) 55.
[38] N. Khan, F. Afaq, M.H. Kweon, K.M. Kim, H. Mukhtar, Cancer Res. 67 (2007) 3475.
[39] O.J. Lowry, N.J. Rosebrough, A.L. Farr, R.J. Randall, J. Biol. Chem. 193 (1951) 265.
[40] J.C. Tobon-Velasco, G. Vazquez-Victoro, M. Macias-Silva, E. Cuevas, S.F. Ali, Free Radical Biol. Med. 53 (2012) 1024.
[41] P.W. Laird, A. Zijderveid, K. Linders, M.A. Rudnicki, R. Jaenisch, A. Berns, Nucleic Acids Res. 19 (1991) 4293.
[42] A.B.P. Lever, Inorganic Electronic Spectroscopy, second ed., Elsevier Science Publishers B.V, Amsterdam, 1984. pp. 553.
[43] (a) R.M. Buchanan, M.S. Mashuta, K.J. Oberhausen, J.F. Richardson, J. Am. Chem. Soc. 111 (1989) 4497;
(b) M.M. Tamizh, K. Mereiter, K. Kirchner, B.R. Bhat, R. Karvembu, Polyhedron 28 (2009) 2157.
[44] S. Bag, P.K. Bhaumik, S. Jana, M. Das, P. Bhowmik, S. Chattopadhyay, Polyhedron 65 (2013) 229.
[45] A. Manna, P. Saha, A. Sarkar, D. Mukhopadhyay, A.K. Bauri, D. Kumar, PLoS ONE 7 (2012) 36938.